

Generation of cold polyatomic molecular ions by ion-atom collisions

Wei-Chen Liang^{1*}, Feng-Dong Jia^{1*}, Fei Wang², Xi Zhang¹,
Yu-Han Wang¹, Jing-Yu Qian¹, Xiao-Qing Hu³,
Yong Wu³, Jian-Guo Wang^{3†}, Ping Xue^{2‡} and Zhi-Ping Zhong^{1,4§}

¹School of Physical Sciences, University of Chinese Academy of Sciences,
Beijing, 100049, People's Republic of China

²State Key Laboratory of Low-Dimensional Quantum Physics,
Department of Physics, Tsinghua University,
Beijing, 100084, People's Republic of China

³Institute of Applied Physics and Computational Mathematics,
Beijing 100088, People's Republic of China

⁴CAS Center for Excellence in Topological Quantum Computation,
University of Chinese Academy of Sciences,
Beijing, 100190, People's Republic of China

[†]E-mail: wang_jianguo@iapcm.ac.cn.

[‡]E-mail: xuep@tsinghua.edu.cn.

[§]E-mail: zpzhong@ucas.ac.cn.

*These authors contributed equally to this work.

A goal of studies on ultracold chemical reactions is the formation of ultracold molecules containing three or more atoms. Although the first ultracold polyatomic molecules were formed recently; knowledge of the kinetics of poly-

atomic molecular ions as reaction products remains limited. Thus, we studied ion-atom reaction collisions in a continuous-wave (CW) laser photoionization of cold atoms in an Rb-Rb⁺ hybrid trap. A series of polyatomic molecular ions was produced, with precise changes in the atomic number of one rubidium atom. Using resonant-excitation mass spectrometry, we directly observed Rb₃⁺ and Rb₄⁺ molecular ions in time-of-flight mass spectrum for the first time. The information of the quantum state of these polyatomic molecular ions and the influence factors was obtained by measuring their lifetimes. The approach is simple, robust, and suitable for all types of laser-coolable elements. Our work paves the way for ultracold ion-atom chemical reactions, introduces the concept of polyatomic molecular ion platforms, and deepens the understanding of ion-atom reaction collisions. It has important implications for astronomical sciences, ultracold neutral plasma, cluster physics, and other disciplines.

Introduction

Over the past two decades, researchers have made significant progress in the study of inelastic collisions and reactions using cold hybrid ion-atom systems. While preliminary research has focused on all-neutral chemistry, the current interest is in the study of charged-neutral reactions (1–5) as available techniques allow for the probing of a broader range of energy and species (6–8) as well as trapping and studying reaction products (9, 10). The triatomic molecular ion H₃⁺ is the most abundant charged molecule. It is a unique product of ion-atom chemical reactions and is considered to play a crucial role in the early astrochemistry responsible for the formation of stars (11). As hydrogen-like species, alkali atoms, and ions share common characteristics with hydrogen atoms and ions, the existence of H₃⁺ suggests the presence of alkali metal X₃⁺ molecular ions, and the possibility has been theoretically verified (12). As the

interaction potential follows the relation $V(r) \propto -1/r^4$ (r is the internuclear distance), it is also expected that a large cross-sectional reaction occurs between diatomic molecular ions and atoms (12, 13). This suggests that the experimental investigation and application of alkali metal X_3^+ should be possible in experiments with cold ion-atom mixtures. While studies on reactive collisions between molecular ions and atoms have been extensively conducted (12–14), no experimental observation of alkali metal X_3^+ molecular ions has been reported yet. Furthermore, the measurement of reaction rates and other kinetic properties has not been reported.

Currently, reactive two-body collision coefficients or cross sections for atomic ion-atom systems have only been determined experimentally for alkaline-earth or alkali-metal heteronuclear systems (1, 2, 15–23). The difference in the measured reaction-rate coefficients of these heteronuclear systems varies in a wide range of 10^{-10} cm³/s to 10^{-13} cm³/s (1, 2, 16–18, 20, 21, 23). Furthermore, no two-body reaction rate coefficient has yet been reported for homonuclear systems. Moreover, in most of these studies, ion-atom reaction rate coefficients are generally determined based on the information of reactants rather than products because the direct measurement of reaction products require a large ensemble of products or advanced techniques, which have been difficult to realize until recent times (15, 22, 24). Dieterle *et al.* (15, 22) used time-of-flight mass spectrometry (TOF-MS) to directly measure the yield of molecular ions and obtained the corresponding three-body reaction rates. However, the TOF spectrum did not reveal the data of the temperature or kinetic energy of the ions because a single-ion ensemble was used in the study. Because previous studies focusing on ion-atom reactions have only provided limited information, the subsequent kinetics of reaction products after reactive collisions largely remains unknown (22, 23).

To address these limitations, we studied ion-atom reactive collisions in a continuous-wave (CW)-laser photoionization of laser-cooled rubidium atoms in an ion-atom hybrid trap. We prepared a series of polyatomic molecular ions guaranteed by the Langevin capture model de-

scribing ion-atom reaction collisions, as shown in Fig.1, in which the number of atoms varies exactly to one atom. We experimentally used the REMS method to directly observe these reaction products. We used two methods to observe the generation of polyatomic molecular ions: (1) Applying an additional radio frequency and continuously scanning the radio frequency. When an ion sample was resonantly excited at the radio frequency, the ion sample was driven away and the intensity decreases, as shown in Fig.2. According to the Langevin model, the reduction in the number of ions was proportional to $1/\sqrt{\mu}$. We measured the amount of Rb_3^+ and found that it was less than the theoretical prediction, which was consistent with the experimental results. This result was due to the influence of the atomic polarizability by the ion sample. The amount of Rb_4^+ ion was closer to the theoretical value. The difference between Rb_3^+ and Rb_4^+ was related to the ion charge distribution. At present, the potential energy curve of the rubidium 4 ion has not yet been calculated. (2) The additional radio frequency could be switched rapidly under the resonance frequency of different ion samples to drive away multiple ions at the same time. As shown in Fig.4, Fig.4(a) shows that the molecular ions were driven away, the atomic ion spectrum peaks moved backward, and the width increased, which indicated that the atomic ions collided with the molecular ions, the energy was concentrated on the atomic ions, the number of molecular ions decreased, and the temperature of the atomic ions decreased. The peak moved back and broadened, and its intensity also increased. Simultaneously, the atomic ions and molecular ions were driven away, leaving only Rb_3^+ and Rb_4^+ , and the area increased because the polyatomic molecular ions collided with ions and dissociated. Meanwhile, the atomic ions Rb_2^+ and Rb_3^+ were driven away, and Rb_4^+ remained. The spectrum analysis results are shown in the figure, which also indicates that the amount of Rb_4^+ is more than that of Rb_3^+ .

We studied the product quantum state and its influencing factors. The quantum state of the product was described by the lifetime. We measured the lifetime of the product to directly obtain the quantum state information of the product, and determined the factors that affected

the quantum state of the product and whether this factor increased or decreased the vibration quantum number. As the vibrational quantum number increased, the product lifetime decreased. (Although the absolute vibration quantum number was not known). We found that six factors affected the product quantum state: (1) Collision energy: The greater the collision energy, the greater the vibration number. This is because the collision energy was high, the energy transmitted in the past was large, the vibration number was high, and the lifetime was short; (2) Initial electron temperature (wavelength of ionizing light): When the initial electron temperature was less than 1000 K, the ion-electron spatial correlation was established, and disorder-induced heating occurred (without plasma, DIH was reduced but still existed), and our results for the diffusion rate coefficient were supported this trend; (3) Number of ions: The number of ions decreased, and ion-ion collisions heated the atomic ions, increasing the collision energy; (4) Secondary collisions: The secondary collision between the atom and the product led to the quenching effect, quenching to a deeper bound state; (5) Proportion of excited state, two reaction channels; (6) Duration of ionizing light: The atomic density and ion density change, and the number of ions decreases. These results help improve the understanding of the dynamics in ion-atom reactive collisions, revealing new possibilities to test fundamental physics and chemistry, which can help precisely manipulate inter-particle interactions for various other applications.

Experimental approach

Our experiments started with the preparation of cold Rb atoms. The experimental apparatus has been introduced in Ref. (7). In brief, $5\text{-}10 \times 10^7$ cold Rb atoms were loaded into the MOT with a temperature of ~ 0.2 mK and an atomic density of 10^{11} cm^{-3} . About 68 % of cold atoms were in the ground state $|5S_{1/2}\rangle$, and 32 % were in the excited state $|5P_{3/2}\rangle$ as the intensity of cooling laser was ~ 49.9 mW/cm^2 (25). Rb^+ ions were generated by the two-step CW-laser photoionization of cold Rb atoms. Briefly, the MOT cooling laser excited the Rb atoms from the ground

state $|5S_{1/2}\rangle$ to the excited state $|5P_{3/2}\rangle$, then the ionizing laser with adjustable wavelength and intensity ionized the Rb atoms at $|5P_{3/2}\rangle$ state to produce Rb^+ ions. The effective intensity of the ionizing laser was reasonably represented by the loss rate of Rb atoms during photoionization, e.g., γ_x , as discussed in Ref. (26). Rb_2^+ , Rb_3^+ and Rb_4^+ polyatomic molecular ions were produced in the MOT (see Appendices for detail) through spontaneous radiative association between Rb^+ , Rb_2^+ and Rb_3^+ ions and Rb atoms, respectively (12, 13) during photoionization, as seen in Fig.1. The ion trap was simultaneously switched on to store ions. It was operated at a radio frequency (RF) of $\Omega_{RF} = 2\pi \times 550$ kHz with an amplitude of $V_{trap} = 140$ V, and the distance between two proximate rod electrodes was $r_0 = 15$ mm. The radial secular frequencies ω_r for the trapped Rb^+ , Rb_2^+ , Rb_3^+ , and Rb_4^+ are $2\pi \times 109.2$ kHz, $2\pi \times 54.6$ kHz, $2\pi \times 36.9$ kHz, and $2\pi \times 22.5$ kHz, respectively.

We used time-of-flight mass spectrometry (TOF-MS) to detect ions (7, 8). The TOF-MS technique can distinguish Rb^+ from the ionic mixture but cannot distinguish between Rb_2^+ , Rb_3^+ , and Rb_4^+ . Therefore, we combined it with resonant-excitation mass spectrometry (REMS) to distinguish Rb_3^+ and Rb_4^+ by applying an additional RF field with an amplitude of $V_{RF} = 4$ V. When the additional RF field is in the vicinity of the radial secular frequencies of the trapped ions, it can excite the motion of ions and drive the ions out of the trap (see Fig.1) (27).

Formation of polyatomic molecular ions

We first demonstrated that the formation of a set of polyatomic molecular ions was in agreement with the Langevin-capture model. Then, we directly observed polyatomic molecular ions by resonant-excitation mass spectrometry. As discussed above, the resonant frequencies (secular frequencies) for Rb^+ , Rb_2^+ , Rb_3^+ , and Rb_4^+ are $2\pi \times 109.2$ kHz, $2\pi \times 54.6$ kHz, $2\pi \times 36.9$ kHz, and $2\pi \times 22.5$ kHz, respectively. We used two methods. In the first approach, only a specific ion was driven away by applying the additional RF. When its frequency caused ion resonance

excitation, these ions were driven away from the ion trap, resulting in a decrease in the intensity of the corresponding position peak in TOF-MS, as seen in Fig.2. The second approach involved quickly switching additional RF frequencies and simultaneously driving away multiple ions.

Fig.3 demonstrates the first approach. Clearly, as the additional RF frequency varied, the spectral peak intensity decreased at the resonance frequency. The ratio of the decreased area to the total area satisfied the Langevin-capture model, which was inversely proportional to the reduced mass of this ion and atom. Rb_2^+ and Rb_4^+ were expected to be close to the Langevin capture model, but Rb_3^+ was significantly smaller than theoretical expectations. We speculate that the reason is the one described in Ref. (28). Studies have shown that atomic polarizability is related to the distribution of ion charges. The Langevin-capture model is suitable for ion charge distribution with a spherical shape. If the ion charge distribution deviates from the spherical shape, the reaction rate coefficient is smaller than that corresponding to the Langevin-capture model. This is a good explanation for our experimental results: The charge distribution of Rb^+ ions was spherical; thus, the reaction rate coefficient of rubidium molecular ions was close to the expectation of the Langevin-capture model. The low reaction rate of Rb_3^+ ions was due to the linear nature of Rb_2^+ , which significantly deviated from the spherical shape (28). The geometric configuration of Rb_3^+ was triangular (12) and closer to spherical shape; thus, the reaction rate coefficient of Rb_4^+ was close to that of the expected Langevin-capture model.

Fig.4 demonstrates the second approach. We first applied a $2\pi \times 46.0$ kHz RF field for $2000 \mu\text{s}$ to exclude Rb_2^+ , as shown in Fig.4(a). Then, we quickly switched the frequency to $2\pi \times 109.2$ kHz and maintained the RF field for $200 \mu\text{s}$ to exclude Rb_2^+ . Consequently, only Rb_3^+ and Rb_4^+ remained in the ionic mixture (see Fig.4(b)). Next, we switched the frequency to $2\pi \times 31.0$ kHz and maintained the RF field for $4000 \mu\text{s}$ to exclude Rb_3^+ . The remaining ions were Rb_4^+ , as shown in Fig.4(c). We found that when Rb^+ and Rb_2^+ were removed from the ionic mixture, the number of Rb_3^+ and Rb_4^+ was less than the case when both Rb^+ and Rb_2^+ are present in the mixture.

This proved that the dissociation of Rb_2^+ , Rb_3^+ , and Rb_4^+ molecular ions was due to Coulomb collisions between different ion species. Moreover, these results showed that the number of Rb_4^+ was greater than that of Rb_3^+ , which was in agreement with the observation made using the first approach.

We now demonstrate how to directly distinguish Rb_3^+ and Rb_4^+ through the TOF spectrum. The ionic mixture was first prepared by photoionizing Rb atoms. Then, an additional RF field with $\omega_{RF} = 2\pi \times 109.2$ kHz was applied to heat and expel Rb^+ , and the TOF spectrum of the remaining ions was then recorded. The TOF spectra obtained with and without RF heating were obtained and compared. As shown in Fig.2, the amount of Rb_2^+ , Rb_3^+ , and Rb_4^+ in the ionic mixture remained high when Rb^+ escaped from the mixture after heating. This indicates that the dissociation of Rb_2^+ and Rb_3^+ is mainly due to inelastic Coulomb collisions. After heating the ions with an RF field, the number of Rb^+ significantly decreased. The ratio of the signal intensity of Rb^+ , Rb_2^+ , Rb_3^+ , and Rb_4^+ changed; therefore, the synthesized curve of TOF spectrum showed three respective peaks. Because different time-of-flight spectra represent different ionic species, it can be judged that the three peaks are attributed to Rb^+ , Rb_2^+ , and $\text{Rb}_3^+ + \text{Rb}_4^+$ because the amount of Rb_4^+ was small compared to that of the other ions.

Quantum state of reaction products and affecting factors

The quantum state of the products is characterized by their lifetime. We measured the lifetime of reaction products to directly obtain information about the quantum state of the products and reveal the factors that affected these state. We also determined whether one factor resulted in the increase or decrease in the vibrational number.

Each experimental cycle for lifetime measurement consisted of five steps in the following sequence: (1) loading the MOT to steady state; (2) simultaneously switching on the ionizing laser and ion trap and keeping them operating for a predetermined duration; (3) switching off

the ionizing laser and MOT to exclude atoms while keep the ion trap operating; (4) trapping the ions for a predetermined period; (5) at the end of the hold time, switching off the ion trap and extracting the ion TOF spectrum. The hold time was varied and the sequence was repeated. Therefore, we obtained the number of ions as a function of hold time in the trap. Fitting the decay in the number of molecular ions with a single exponential decay function resulted in the dissociation of the lifetime of the molecular ions.

We simulate the experiment measurement to establish a rate-equation model containing number of atoms and ions (?). By fitting the rate equations to the experimental data ,the dissociation lifetime of polyatomic ions are obtained. The measured typical lifetime of Rb_2^+ , Rb_3^+ and Rb_4^+ were 7500 ms, 300 ms and 150 ms, respectively. The reciprocal of the FWHM of the tof peak of a particular ion in the MOT represent its temperature (8). Noted that there is no DIH and the atomic ion temperature is mK when the starting electron temperature is greater than 1000 K , (26, 31) . As a result, the temperature of the Rb^+ is about mK as the ionizing light's wavelength is 447 nm, and the typical temperatures for Rb^+ , Rb_2^+ , are 20 mK, respectively.

We performed the lifetime measurement of Rb_2^+ as an example since the amount of Rb_2^+ was the largest. The lifetime of Rb_2^+ and the seven influencing factors are shown in Fig.6. The seven influencing factors and the corresponding physical mechanisms are explained as follows:

(1) Collision energy which is determined by ion kinetic energy, ion kinetic energy is characterized by the full-width at half-maximum (FWHM) of its corresponding peak in the TOF spectrum (The ion kinetic energy is inversely proportional to the FWHM of its spectral peak in the TOF). As shown in Fig.6(a), our measurements demonstrated that The larger the collision energy was, the shorter the product life was, i.e., the vibration quantum number increased. This indicated that the internal and kinetic energy of Rb_2^+ was transferred from collision energy, e.g., $E_{col} = E_k(\text{Rb}_2^+) + E_{vib.}(\text{Rb}_2^+)$. This was consistent with the results in Ref. (29, 30). However, the collision energy in our experiments was in 10 mK-K range (see Appendices) which was

considerably lower than that in Ref. (29), e.g., about 74418 K (6.40 eV).

(2) The initial electron temperature (wavelength of the ionizing laser). As shown in Fig.6(b), the lifetime of the product with an ionized light wavelength of 447 nm was greater than that of the product with an ionized light wavelength of 478.8 nm. Note that this comparison was made when the two ionized light intensities (characterized by atomic loss rate γ_x) were almost the same. Our results suggested it was due to the disorder-induced heating (DIH) of ions. According to the research results of UNP (31–33), DIH caused by electron ion spatial correlation in quickly heated the ions to a few K in microseconds. Ultracold plasma can only be generated when the wavelength of ionized light is less than 1000 nm. For our experiment, the wavelength of 478.8447nm ionization light corresponded to the initial electron temperature respectively. The kinetic energy of ions was high and the collision energy was larger. As before, more collision energy was transferred to the product, which increased its vibration quantum number and shortened its lifetime. This was further proved in our study on the diffusion rate of ions (?).

(3) Atomic density. As shown in Fig.6(c), when the atomic density was higher, the lifetime of molecular ions was longer. We believe it was because molecular ions would quench into deeper-bound vibrational state in the secondary molecular ion-atom collisions. This is so-called vibrational quenching effect (14, 34), resulting in a longer lifetime of molecular ions.

(4) The fraction of Rb atoms in the $|5P_{3/2}\rangle$ state. As shown in the Fig.5, both the atomic ground state and the atomic excited state could react and collide with ions as a result, The proportion of atomic excited state affected the quantum state of the product.

(5) Intensity of ionizing laser which represented by the atomic loss rate γ_x . When γ_x was larger, the density of remaining atoms was lower after a same period of photoionization. The reason was that the ionizing light was strong, the atomic density was small, and the quenching effect was weak(see Fig.6(d)).

(6) The number of total ions. As shown in Fig.6(e), the more total ions, the shorter the

product lifetime. This was because ionic mixture systems concentrated energy on lighter elements (33). When there were less Rb^+ , there would be less Coulomb collisions between Rb^+ and Rb_2^+ . Therefore, the lifetime of molecular ions was expected to be longer (see Fig.6(e)).

(7) Duration of the photoionization. The density of atoms and number of Rb^+ were continuously varying during the photoionization. Both of atomic density and number of Rb^+ affected the lifetime of molecular ions.

Note that these seven factors are not independent, the situation becomes more complicated when other factors are at play.

Conclusion

Based on Rb-Rb^+ hybrid trap, we investigated ion-atom reaction collisions in the continuous photoionization process of cold atoms. We generated a set of polyatomic molecular ions, with precise changes in the atomic number of one rubidium atom. We directly observed Rb_3^+ and Rb_4^+ by two approaches based on resonant-excitation mass spectrometry. Our approach is simple, robust (ensured by Langevin-capture theory), and universal i.e., suitable for all types of laser-coolable elements. Furthermore, we examined the subsequent kinetics of polyatomic molecular ions. We directly determined the quantum states of polyatomic molecular ions through lifetime measurements. We found seven factors that affect the quantum states of products and how they affect them, and we revealed the underlying physical mechanisms.

These results provide a direct insight on the dynamics in ion-atom reactive collisions. They also provide tools for studying quantum few-body problems and pave the way for the study of atomic processes in astrophysics, ultracold plasmas, and other fields. The influence of electrons on the quantum states of reaction products opens new directions for the study of atomic processes in ultracold plasmas. This work serves as an important reference for the study of high-energy-density plasmas.

Figure 1: Schematic diagram of the formation of a series of rubidium polyatomic molecular ions, and precise changes in a rubidium atom according to the Langevin-capture model.

Acknowledgments

This study was supported by the National Key Research and Development Program of China (Grant Nos. 2017YFA0402300 and 2017YFA0304900), the Beijing Natural Science Foundation (Grant No. 1212014), Fundamental Research Funds for the Central Universities, the Key Research Program of the Chinese Academy of Sciences (Grant No. XDPB08-3), specialized research fund for CAS Key Laboratory of Geospace Environment (Grant No. GE2020-01), and National Natural Science Foundation of China (Grant Nos. 61975091, 61575108).

References

1. F. H. Hall, M. Aymar, M. Raoult, O. Dulieu, S. Willitsch, *Molecular Physics* **111**, 1683 (2013).
2. W. G. Rellergert, *et al.*, *Physical Review Letters* **107**, 243201 (2011).
3. O. Dulieu, A. Osterwalder, *Cold Chemistry: Molecular Scattering and Reactivity Near Absolute Zero* (The Royal Society of Chemistry, 2017).
4. L. Ratschbacher, C. Zipkes, C. Sias, M. Köhl, *Nature Physics* **8**, 649 (2012).
5. T. Sikorsky, Z. Meir, R. Ben-shlomi, N. Akerman, R. Ozeri, *Nature Communications* **9**, 920 (2018).
6. M. Beyer, F. Merkt, *Physical Review X* **8**, 031085 (2018).
7. S.-F. Lv, *et al.*, *Chinese Physics Letters* **34**, 013401 (2017).

8. W.-C. Liang, *et al.*, *Acta Physica Sinica* **72**, 0 (2023).
9. P. Puri, *et al.*, *Nature Chemistry* **11**, 615 (2019).
10. S. J. Schowalter, K. Chen, W. G. Rellergert, S. T. Sullivan, E. R. Hudson, *Review of Scientific Instruments* **83**, 043103 (2012).
11. T. González-Lezana, P. Honvault, *International Reviews in Physical Chemistry* **33**, 371 (2014).
12. M. Śmiałkowski, M. Tomza, *Physical Review A* **101**, 012501 (2020).
13. M. Tomza, *et al.*, *Reviews of Modern Physics* **91**, 035001 (2019).
14. J. Pérez-Ríos, *Physical Review A* **99**, 022707 (2019).
15. T. Dieterle, *et al.*, *Physical Review Letters* **126**, 033401 (2021).
16. F. H. J. Hall, M. Aymar, N. Bouloufa-Maafa, O. Dulieu, S. Willitsch, *Physical Review Letters* **107**, 243202 (2011).
17. F. H. J. Hall, *et al.*, *Molecular Physics* **111**, 2020 (2013). ArXiv:1302.4682 [physics].
18. S. T. Sullivan, W. G. Rellergert, S. Kotochigova, E. R. Hudson, *Physical Review Letters* **109**, 223002 (2012).
19. A. Härter, *et al.*, *Physical Review Letters* **109**, 123201 (2012).
20. A. Krüchow, *et al.*, *Physical Review Letters* **116**, 193201 (2016).
21. A. Krüchow, A. Mohammadi, A. Härter, J. Hecker Denschlag, *Physical Review A* **94**, 030701 (2016).
22. T. Dieterle, *et al.*, *Physical Review A* **102**, 041301 (2020).

23. A. Mohammadi, *et al.*, *Physical Review Research* **3**, 013196 (2021).
24. M.-G. Hu, *et al.*, *Science* **366**, 1111 (2019).
25. W. Huang, *et al.*, *Chinese Physics Letters* **29**, 013201 (2012).
26. F. Wang, *et al.* (2023).
27. K. Ravi, S. Lee, A. Sharma, G. Werth, S. A. Rangwala, *Applied Physics B* **107**, 971 (2012).
28. A. D. Dörfler, *et al.*, *Nature Communications* **10**, 5429 (2019).
29. M.-M. He, J. Hu, C.-X. Wu, Y. Zhi, S. X. Tian, *The Journal of Physical Chemistry A* **124**, 3358 (2020).
30. J. Pérez-Ríos, *Physical Review A* **104**, L031302 (2021).
31. T. Killian, T. Pattard, T. Pohl, J. Rost, *Physics Reports* **449**, 77 (2007).
32. M. Lyon, S. L. Rolston, *Reports on Progress in Physics* **80**, 017001 (2017).
33. R. T. Sprenkle, L. G. Silvestri, M. S. Murillo, S. D. Bergeson, *Nature Communications* **13**, 15 (2022).
34. K. Jachymski, F. Meinert, *Applied Sciences* **10**, 2371 (2020).
35. S. Jyothi, *et al.*, *Physical Review Letters* **117**, 213002 (2016).
36. H. Hirzler, E. Trimby, R. Gerritsma, A. Safavi-Naini, J. Pérez-Ríos, *Phys. Rev. Lett.* **130**, 143003 (2023).
37. D. W. Sesko, T. G. Walker, C. E. Wieman, *J. Opt. Soc. Am. B* **8**, 946 (1991).

38. X.-K. Li, *et al.*, *Journal of Physics B: Atomic, Molecular and Optical Physics* **53**, 219501 (2020).
39. Y.-P. Ruan, *et al.*, *Chinese Physics Letters* **31**, 073401 (2014).

Acknowledgments

Include acknowledgments of funding, any patents pending, where raw data for the paper are deposited, etc.

Supplementary materials

Materials and Methods

Supplementary Text

Figs. S1 to S3

Tables S1 to S4

References (4-10)

0.1 Methods

0.1.1 Preparation of atoms and ions

The first excitation laser was the MOT cooling laser with a detuning of 12 MHz of the transition $5^2S_{1/2}, F = 2 \rightarrow 5^2P_{3/2}, F' = 3$. The second excitation laser, that is, ionization laser, was provided by another cw-diode laser. The ionizing laser has variable intensity and wavelength. The ionizing laser and ion trap were kept on for a 750-ms duration. During the photoionization, Rb_2^+ , Rb_3^+ and Rb_4^+ molecular ions were created through spontaneous radiative association between Rb^+ , Rb_2^+ and Rb_3^+ ions and Rb atoms (12, 13, 35, 36), respectively, as shown in Fig.1. Therefore, a mixture of Rb^+ , Rb_2^+ , Rb_3^+ and Rb_4^+ was created. These ions are separated as MOT

ions and LPT ions because the density and of ions in LPT ion cloud is much lower than that in MOT ion cloud and the size of LPT ion cloud is much larger than MOT cloud containing ions and atoms. As seen in Fig.7, after a fixed period of photoionizing atoms, the ionizing laser was switched off and LPT was kept on, the yield of reaction products remains unchanged whether the MOT was switched on or off after trapping the ions for a period. This means reactive collision scarcely happens between LPT ions and atoms and only takes place between MOT ions and atoms.

In our experiments, system parameters are given as follows. The number of atoms and $1/e^2$ half-waist of the cold atomic cloud in MOT were measured as $5 \sim 10 \times 10^7$, $0.5 \sim 1.0$ mm using absorption imaging (37) and the temperature T of atoms was approximately 200μ K. The wavelength of the ionizing laser is variable in the range of $\lambda_{ion} = 447 \sim 478.8$ nm, corresponding to initial electron temperature in the range of $T_e = 1295 \sim 11.2$ K (26). The radial directions x, y, and axial direction z of the ion cloud were 2.7, 2.7, and 25.2 mm, respectively (7). The well-depth of the ion trap was approximately 0.7 eV, corresponding to a maximum temperature ranging at $10^3 - 10^4$ K for the trapped Rb^+ -ion (7, 38). For the ions created in the photoionization of cold atoms, momentum and energy conservation ensured that the initial kinetic energy of the Rb^+ was approximately two orders of magnitude larger than that of the cold atom (39), that is, 20 mK, which were subsequently heated by disorder-induced heating (26,31). As for a typical ultracold neutral plasmas created by photoionizing laser-cooled atoms near the ionization threshold, the effective ion temperature evolved to several 1 K on the timescale of $\sim 10^2$ ns (31), thus the minimum collision energy was approximately 10 mK-K.

0.1.2 Measurement of molecular ions' lifetime

The experimental scheme for reaction product lifetime measurements is: after the period that MOT, the ionization laser and the LPT work together for 1200 ms during which Rb_2^+ molec-

ular ions are formed, then the ionization laser is turned off, ions are trapped in the LPT for a controlled time Whether the mot is working or not. Finally, the LPT is turn off, ions are pushed to the MCP and ion counts are extracted from TOF spectra. the product intensity as the function of ion trap hold time is obtained by changing the hold time of the product in the ion trap, which is a good single exponential decay curve. We fit the curve to obtain the lifetime of product quantum state. Typical experimental measurements are shown in Fig.7. Comparing lifetime measurements Whether the mot is working or not, the two curves are the same within the experimental error, indicating that ion-atom reaction collisions only contribute to ion production by photoionization of cold atoms in the magneto-optical trap, and that ions in the ion trap have no contribution to the ion-atom reaction collisions because of their thin density and high temperature

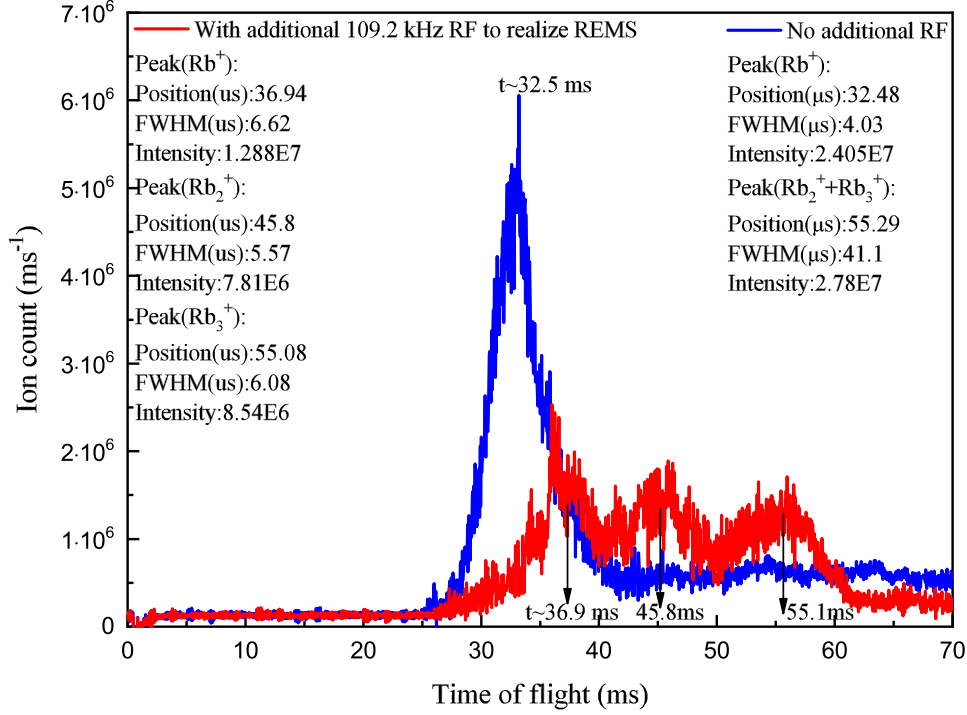


Figure 2: Rb⁺, Rb₂⁺ and Rb₃⁺ were directly observed using resonant-excitation mass spectrometry (REMS), i.e., by applying an additional RF field. The motion of confined ions can be excited upon resonant irradiation; as a result, it was heated and subsequently left the ion trap. Different ion species have different resonant-excitation frequencies. Here, we applied an additional RF with 109.2 kHz, RF amplitude of 4 V was applied for 200 μ s, during which Rb⁺ ions were heated and driven out of the ion trap. The wavelength and intensity of the ionizing laser were $\lambda_{ion.} = 478.8$ nm and $\gamma_x = 2.0$ s⁻¹, respectively, and the duration of photoionization was 750 ms. γ_x is the atom loss rate representing the intensity of the ionization laser. The linear ion trap was operated at a RF frequency $\omega_{RF} \approx 2\pi \times 550$ kHz and $V_{RF,trap}$ 140 V. A DC voltage $V_{end} = 90$ V was applied to the end-cap electrodes.

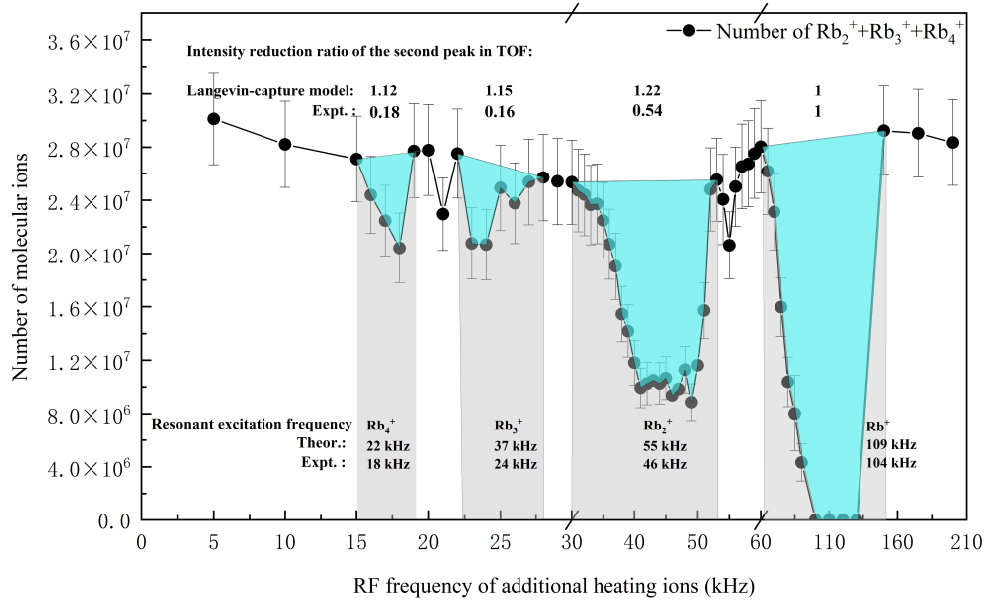


Figure 3: Multiple ions were simultaneously expelled by sweeping the Multiple resonant frequency of the additional RF field. For every experimental cycle, atoms were first loaded into the steady state. Here, the wavelength and intensity of the ionizing laser were $\lambda_{ion.} = 478.8$ nm and $\gamma_x = 2.0 \text{ s}^{-1}$, respectively, and the duration of photoionization was 750 ms. The amplitude of the RF field was 4 V, and the duration of RF heating was $500 \mu\text{s}$.

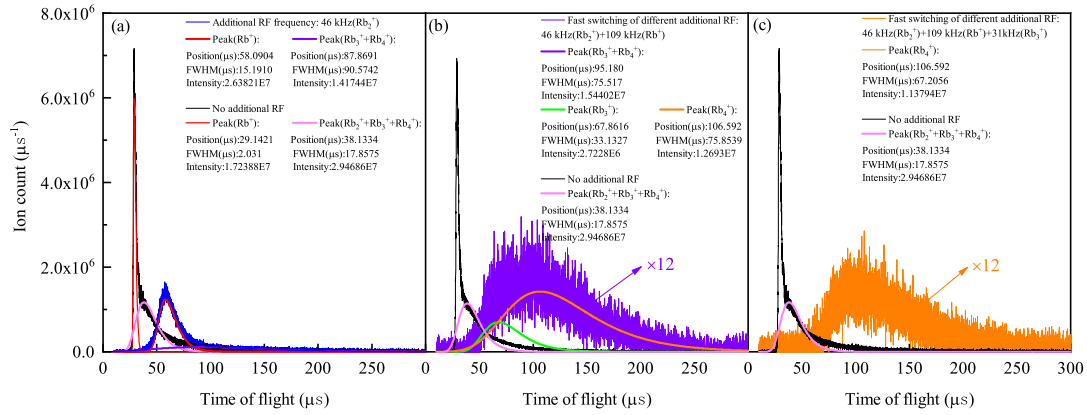


Figure 4: Observing weak Rb_3^+ and Rb_4^+ signal by sweeping the Multiple resonant frequency of the additional RF field: 109.2 (Rb^+), 46.0 (Rb_2^+), and 31.0 kHz (Rb_3^+). The durations of RF heating were 175 μs , 2000 μs , and 4000 μs for 109.2, 46.0, and 31.0 kHz, respectively.

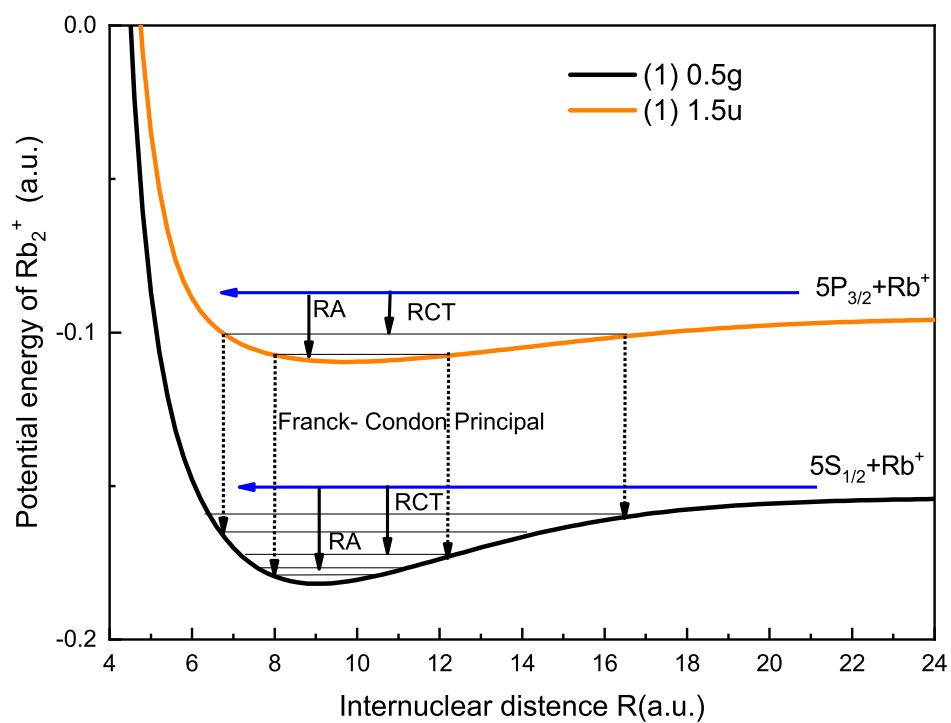


Figure 5: Schematic representation of possible channel of formation of rubidium molecular ion c: RA-radiative association, RCT-radiative charge transfer. The potential curve was calculated by Jyothi *et al.* (35).

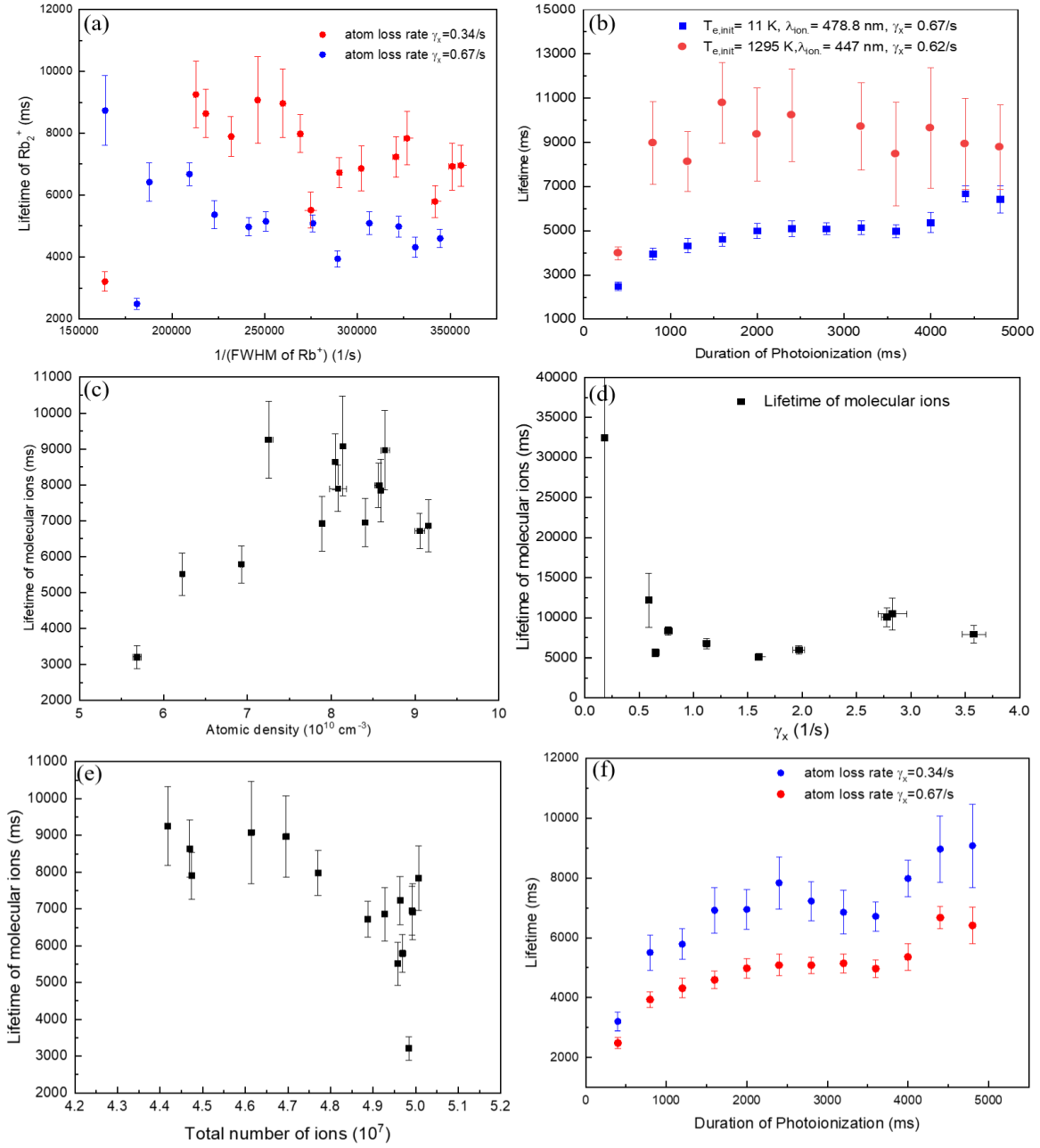


Figure 6: Lifetime and affecting factors of rubidium molecular ions. Here, the wavelength, intensity of the ionizing laser were $\lambda_{\text{ion.}} = 478.8 \text{ nm}$ in (a) and (c)-(f). (a) Collision energy, e.g., kinetic energy of Rb^+ . Here the kinetic energy of Rb^+ is reasonably represented by the inverse of the full-width at half-maximum (FWHM) of its corresponding peak in the TOF spectrum, as discussed in Ref. (8). (b) The wavelength of ionizing laser. (c) Atomic density. (d) Intensity of ionizing laser γ_x . (e) Total number of ions, here the intensity of the ionizing laser was $\gamma_x = 0.34 \text{ s}^{-1}$. (f) Duration of the ionization laser.

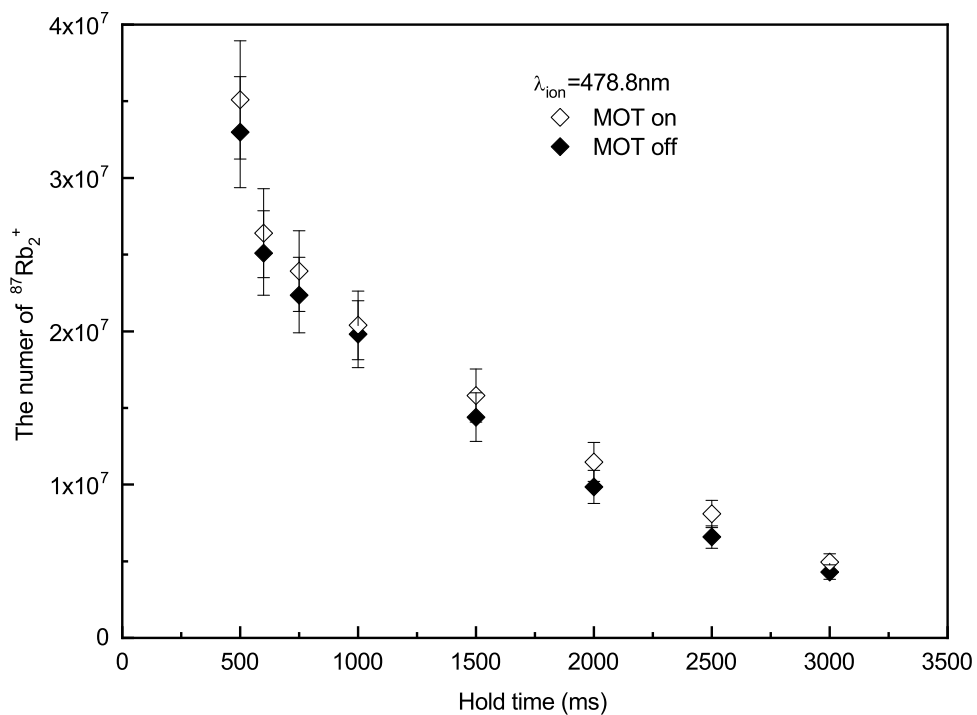


Figure 7: Region of product generation. $\text{Rb}+2$ signal are measured as the function of the hold time whether the MOT is working or not. The time zero is set to the moment when the ionization laser, the gradient magnetic field and the re-pump light are turn off after $\text{Rb}+2$ molecular ions are created. Here, the wavelength, intensity of the ionizing laser were $\lambda_{\text{ion.}} = 478.8 \text{ nm}$, $\gamma_x = 1.34/\text{s}$, respectively and duration of photoionization was 1200 ms.